IOP Conference Series: Earth and Environmental Science

PAPER • **OPEN ACCESS**

Comparison of Land Surface Temperature Derived From Landsat 7 ETM+ and Landsat 8 OLI/TIRS for Drought Monitoring

To cite this article: A S A Nugraha *et al* 2019 *IOP Conf. Ser.: Earth Environ. Sci.* **313** 012041

View the article online for updates and enhancements.

This content was downloaded from IP address 105.160.92.194 on 16/07/2021 at 23:05

IOP Conf. Series: Earth and Environmental Science **313** (2019) 012041 doi:10.1088/1755-1315/313/1/012041

Comparison of Land Surface Temperature Derived From Landsat 7 ETM+ and Landsat 8 OLI/TIRS for Drought Monitoring

A S A Nugraha[1,2], T Gunawan[3] and M Kamal[3]

[1] Postgraduate Program of Remote Sensing, Faculty of Geography, Universitas Gadjah Mada, Yogyakarta, Indonesia.
[2] Department of Geographic Education, Faculty of Law and Social Science, Universitas Pendidikan Ganesha (Undiksha), Bali, Indonesia
[3] Department of Geographic Information Science, Faculty of Geography, Universitas Gadjah Mada, Yogyakarta, Indonesia.

Email: adi.nugraha@undiksha.ac.id

Abstract. The thermal infrared bands of Landsat 7 ETM+ and Landsat 8 OLI/TIRS have ability to provide Land Surface Temperature (LST) information. This information is important to map and monitor Earth surface's temperature-related events such as drought. However, these two Landsat sensors have different conversion methods of deriving LST information from their image pixels. Landsat 7 ETM+ applies a simple algorithm using single thermal band to produce an index of surface temperature; while Landsat 8 TIRS applies two thermal bands and a more sophisticated Split Windows Algorithm (SWA). This research aims to compare and contrast the ability of Landsat 7 ETM+ and Landsat 8 OLI/TIRS to map LST for drought monitoring in part of East Java Province, Indonesia. Drought detection was conducted using two different algorithms, namely Temperature Condition Index (TCI) with a range of values from 0-100 and Crop Water Stress Index (CWSI) with a range of 0-1. These algorithms have an opposite index value explanation; zero in TCI indicates drought condition, but wet condition in CWSI. The differences in the LST results from Landsat images showed that SWA method provides more similar results to the corresponding land cover conditions as compared to the result of Landsat 7 ETM+. Drought detection results demonstrate that TCI and CWSI would be optimally useful for area have a potential drought. Both methods have similar results in terms of the condition of Land Surface Temperatures.

Keywords: *Landsat, Land Surface Temperature, drought, monitoring*

1. Introduction

Changes in Earth's surface land cover have an impact to the changes of the Land Surface Temperature (LST) of a region. The changes in land cover will effect on the atmospheric conditions of a region and the condition of the watersheds, where they have a specific characteristic of the soil, water, and surface flow [1]. This change has implications to the local temperature condition of a region, such as increasing the local temperature of a town due to the expansion of settlements. However, this condition change could also be triggered by global changes caused by climate

Content from this work may be used under the terms of the Creative Commons Attribution 3.0 licence. Any further distribution of this work must maintain attribution to the author(s) and the title of the work, journal citation and DOI.
Published under licence by IOP Publishing Ltd

anomalies such as El-Nino. The climate anomalies will give double impact apart from the land cover changes that is called drought.

Drought in general is a condition where a region experiences a shortage of water supply [2]. Drought monitoring is an indispensable task as a form of emergency action to respond the event of drought more efficiently and rapidly. The vast extent and rapid change of drought give a challenge for the region managers and government to decide an appropriate policy to handle the drought. The advancement of remote sensing sensors and technology provides an option to map and monitor the drought events efficiently over a large area extent. One of the advantages of remote sensing image is its thermal-infrared band that is capable of detecting temperature as a proxy of drought conditions [3,4]. Several methods have been developed for drought mapping and monitoring from remote sensing images. Two of them are Temperature Condition Index (TCI) and Crop Water Stress Index (CWSI) [4,5]. Both algorithms are able to map the distribution and intensity of drought using thermal-infrared band input.

However, not every remote sensing platform has the thermal-infrared bands on their sensor. Some of the remote sensing platform with thermal-infrared bands are National Oceanic and Atmospheric Administration (NOAA), the Moderate Imaging Spectroradiometer (MODIS), Land Satellite (Landsat), and the Advanced Spaceborne Thermal Emission and Reflection Radiometer (ASTER). This research uses Landsat sensors form different generations; Enhanced Thematic Mapper Plus (ETM+) sensor by Landsat 7 and Thermal Infrared Sensors (TIRS) by Landsat 8. Thermal infrared is capable of detecting temperature and used as a basis for monitoring drought. Landsat 7 ETM+ has two thermal bands known as 6.1 channel (low-gain) and 6.2 (high-gain). High-gain thermal band is more accurate for obtaining temperature information than low-gain band due to the closeness value to the real field conditions [6]. On the other hand, the Landsat 8 OLI/TIRS equipped with thermal-infrared band for band 10 and 11. Landsat 8 OLI/TIRS uses both thermal-infrared bands for obtaining land surface temperature information, and thus its method is considered as a more complex as compared to Landsat 7 ETM+ method [7,8].

Further developments in this field show that extraction of land surface temperature can be used as input for drought mapping and monitoring. The differences in image characteristics and LST algorithms of Landsat 7 ETM+ and Landsat 8 OLI/TIRS need to be investigated in order to monitor drought. This research aims to (1) apply the LST algorithm to both Landsat images, (2) map and monitor the drought through TCI and CWSI, and (3) compare and contrast the results from both Landsat sensors. This research is expected to contribute to the application of thermal-infrared bands of Landsat for drought mapping and monitoring in Indonesia.

2. Research Methods

2.1. Research Site

The sites of this research were Tuban, Surabaya, and Probolinggo Regency, East Java Province, Indonesia, which are prone to drought event. These research sites located at 111° 0’ to -114°4’ East Longitude and 7°12’ to -8°48’ South Latitude (Figure 1). From meteorological records, the average temperature of these regions are increasing every year, to about 0.80°C for Probolinggo Regency, 0.86°C for Tuban Regency, and 0.93°C for Surabaya City. The increasing average temperature resulted in low precipitation rate in these areas. Almost all regions in East Java Province have drought started on May 2015 because of the impact from El-Nino and the temperature increased until November. The drought has impacted unsuccessful harvest in agriculture lands throughout these areas (Table 1) [9].

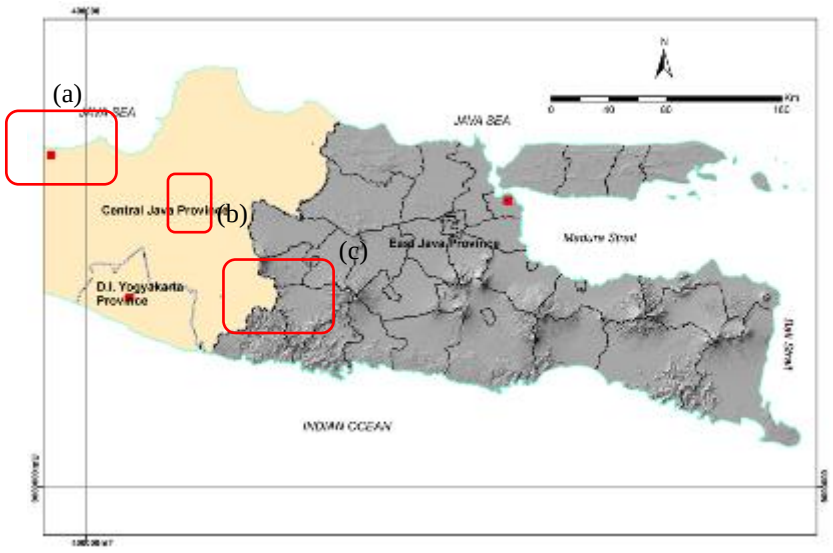

Figure 1. Research locations in East Java Province; (a) Surabaya City, (b) Tuban Regency, and (c) Probolinggo Regency.

Tuban is a structural landform area with many karst (limestone) locations. Surabaya is a highly populated and highly developed area; it has marine originated landform which bordering the sea. Probolinggo is an area that has the most dominant volcanic landform origin in the region [9]. Topographic variations of the three sites are expected to contribute to the results of surface temperature derivation from both Landsat 7 ETM+ and Landsat 8 OLI/TIRS.

Table 1. Agriculture land impacted by drought.

Year	Agriculture Land (Ha)
2012	13.956, 47
2013	257
2014	533
2015	788,8 (Update Agustus 2015)

Source: Bappeda East Java

2.2. Landsat Images

Landsat images used in this research were obtained from two different sensors, Landsat 7 ETM+ and Landsat 8 OLI/TIRS (Table 2). Landsat 7 ETM+ has thermal-infrared band on channel 6.1 (high-gain) and 6.2 (low-gain), where information on the appearance of the land surface temperature is obtained using channel 6.2 because it has accurate results closer to the surface temperature of objects on the ground [6]. Landsat 8 OLI/TIRS has 11 bands and two of them are thermal-infrared bands (band 10 and 11). Landsat images are freely accessible from its official website http://usgs.gov/. This study used Landsat images from year 2002/2003 and 2014/2015 in October, November, and January. Before processing for Landsat 7 ETM+ and 8 OLI/TIRS have been used, there are some correction such as geometric correction, radiometric correction, and atmospheric correction [10]. Radiometric correction is the change of the pixel value to become radiance and reflectance value for all image of them (except thermal band only process to radiance correction) and the result given true pixel value in image. Then, the next step is atmospheric correction using relative methods called Dark Object Subtraction (DOS) where it is committed by decreasing pixel value from dark pixel value on the result of image [11].

Table 2. Landsat image characteristics used in this research.

Characteristics	Landsat 7 ETM+	Landsat 8 OLI/TIRS
Band number	**30 m:** Band 1 - Blue Band 2 - Red Band 3 - Green Band 4 - NIR Band 5 - SWIR-1 Band 7 - SWIR-2 **15 m:** Band 8 - Pan **60 m:** Band 6 - TIR	**30 m:** Band 1 - Coastal aerosol Band 2 - Blue Band 3 - Red Band 4 - Green Band 5 - NIR Band 6 - SWIR-1 Band 7 - SWIR-2 Band 9 – Cirrus **15 m:** Band 8 - Pan **100 m:** Band 10 - TIR-1 Band 11 - TIR-2
Thermal band spectral range	Band 6 (10,31-12,36 nm)	Band 10 (10,60 - 11,19 nm) Band 11 (11,50 - 12,51 nm)
Acquisition dates	- 01 October 2002 - 11 November 2002 - 14 January 2003	- 03 October 2014 - 04 November 2014 - 07 January 2015

Source: NASA 2003, USGS 2015

2.3. Land Surface Temperature Extraction

2.3.1. Landsat 7 ETM+

The extraction of LST information from Landsat 7 ETM+ was conducted using an algorithm that has been mentioned in the Handbook of Landsat 7 ETM+. This algorithm consists of series of sequences that must be undertaken starting from changing the pixel values into radiance values, converting the radiance into temperature brightness, and finally converting the temperature brightness into kinetic temperature (LST). The algorithms used are shown in Equation 1 and 2 below.

$$L\lambda = ((LMAX\lambda - LMIN\lambda)/(QCALMAX-QCALMIN)) * (QCAL-QCALMIN) + LMIN\lambda \quad (1)$$

$$T = K_2 / \ln (K_1/L_\lambda + 1) \quad (2)$$

Where LMAX and LMIN are spectral values contained in the metadata of Landsat images. The calibration values of pixels for QCALMAX and QCALMIN can be found from Landsat image metadata. K_1 and K_2 are predetermined constants values, and $L\lambda$ is the spectral radiance value of the image. The final result from these algorithms is surface temperature brightness information.

2.3.2. Landsat 8 OLI/TIRS

The LST extraction in Landsat 8 OLI/TIRS used a Split Windows Algorithm (SWA) algorithm that was developed. This algorithm was previously applied for LST derivation from NOAA AVHRR weather images. The challenge in using this algorithm is that water vapor and emissivity values need to be determined prior to the implementation of the algorithm (Equation 3).

$$Ts = A_0+A_1*T_{10}-A_2*T_{11} \quad (3)$$

T_{10} and T_{11} are the results of temperature brightness which was obtained from band 10 and band 11 of Landsat 8. The values of A_0, A_1, and A_2 are the results of decreasing value of the information obtained from the transmission atmospheric water vapor and particular emissivity value [12]. The sequence of algorithms used in SWA method can be seen on the Table 3.

Table 3. The sequence of equations for SWA.

Order	Equations	Remark
a	$C_{10} = \varepsilon * \tau_{10}$	ε : image emissivity τ : atmospheric transmission
b	$C_{11} = \varepsilon * \tau_{11}$	
c	$D_{10} = (1 - \tau_{10}) * (1 + (1 - \varepsilon) * \tau_{10})$	
d	$D_{11} = (1 - \tau_{11}) * (1 + (1 - \varepsilon) * \tau_{11})$	
e	$E_0 = D_{11}*C_{10} - D_{10}*C_{11}$	Refer to results of **a**-**b**
f	$E_1 = D_{11}*(1-C_{10}-D_{10})/E_0$	Refer to results of **a**-**e**
g	$E_2 = D_{10}*(1-C_{11}-D_{11})/E_0$	Refer to results of **a**-**e**
h	$A = D_{10}/E_0$	Refer to results of **c**-**e**
i	$A_0 = E_1*a_{10}+E_2*a_{11}$	Refer to results of **f**-**g**
j	$A_1 = 1+A+E_1*b_{10}$	Refer to results of **f**-**h**
k	$A_2 = A+E_2*b_{11}$	Refer to results of **g**-**h**

2.4. Drought Estimation Methods

Land surface temperature (LST) estimation is one of the steps to determine the drought on the Earth's surface. This information can be derived from remote sensing images using algorithms that are specifically developed to provide information related to the dryness of Earth's surface. Temperature Condition Index (TCI) and Crop Water Stress Index (CWSI) are among algorithms developed for this purpose, and are specifically designed for Landsat 7 ETM+ and 8 OLI/TIRS, respectively.

TCI is an algorithm developed by Kogan *et al*. (1997) for detecting drought by viewing the difference from the surface temperatures level resulting in water-saturated soil which affects vegetation stress level (Equation 4). On the other hand, CWSI is an algorithm for detecting drought with a canopy cover approaches that have lost water due to evapotranspiration [5] (Equation 5). TCI has a value range of 0-100 and CWSI has a value range of 0-1. These algorithms have an opposite index value explanation; zero in TCI indicates drought condition, but wet condition in CWSI.

$$TCI = (LSTmax-LST/LSTmax-LSTmin)*100 \quad (4)$$

$$CWSI = LST-LSTmin/LSTmax-LSTmin \quad (5)$$

2.5. Drought Monitoring

To monitor the drought, the land surface temperature information were derived from Landsat 7 ETM+ and 8 OLI/TIRS to visualize the spread of land surface temperature value in the research sites. The land surface temperature value serves as indicator of drought event, and potentially assists the drought monitoring by observing the temperature variations from the map results. High surface temperature values have positive correlation with drought event in an area, and negative correlation with wet condition. Therefore, the applicability of TCI and CWSI methods were tested for drought monitoring.

3. Results and Discussions

3.1. Land Surface Temperature from Landsat Images.

Land Surface Temperature processing of Landsat 7 ETM+ and 8 OLI/TIRS concern about the condition of land cover as a particular emissivity to determine the value of the surface temperature of each object recorded by the image. The land surface temperature value generated by Landsat is a value of land surface temperature which has been recorded. Therefore it cannot become a reference as a standard to reflect the average value.

The range values of land surface temperature of both images are different (° Kelvin), it can be also seen in Figure 2, Figure 3 and Table 4 which show that in the same location and area, those who have higher land surface temperatures and a few other locations have lower temperature. The white

color indicates that the areas have very low temperatures with land cover such as; body of water, shadows, or clouds. It is very difficult to ascertain the difference of the results by only viewing from surface temperature value aspect. Therefore, the difference in the land surface temperature value will be easily noticed when it is associated with land cover of each of the objects that exist, even though it is not an absolute reference.

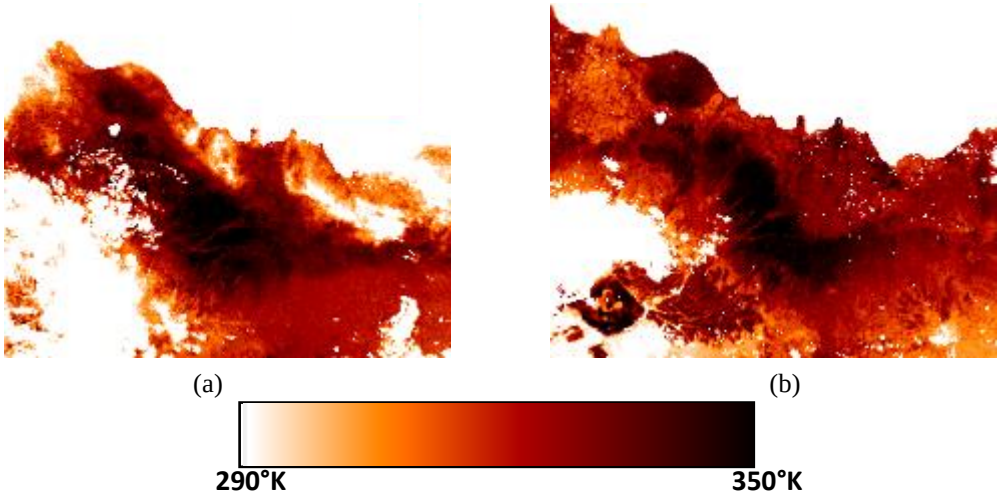

Figure 2. Results of Land Surface Temperature in Purbolinggo; (a) Landsat 7 ETM+ (11 November 2002) and (b) Landsat 8 OLI TIRS (04 November 2014).

Table 4. Land Surface Temperature Value Differences for Each Land cover on Landsat.

No	Land cover classes	Land Surface Temperature of Landsat Images (°K)		Temperature Different (°K)
		ETM+	OLI/TIRS	
1.	Water Bodies (Pond)	292.34	297.63	5.29
2.	Water Bodies (Water puddle on agricultural land)	302.57	300.04	2.55
3.	Low Density Vegetation	293.89	305.51	11.62
4.	Medium Density Vegetation	309.00	303.01	5.99
5.	High Density Vegetation	299.61	293.91	5.7
6.	Built-up Area	305.86	302.13	3.73
7.	Open field	329.99	316.91	13.08

Source: Data Processing 2016.

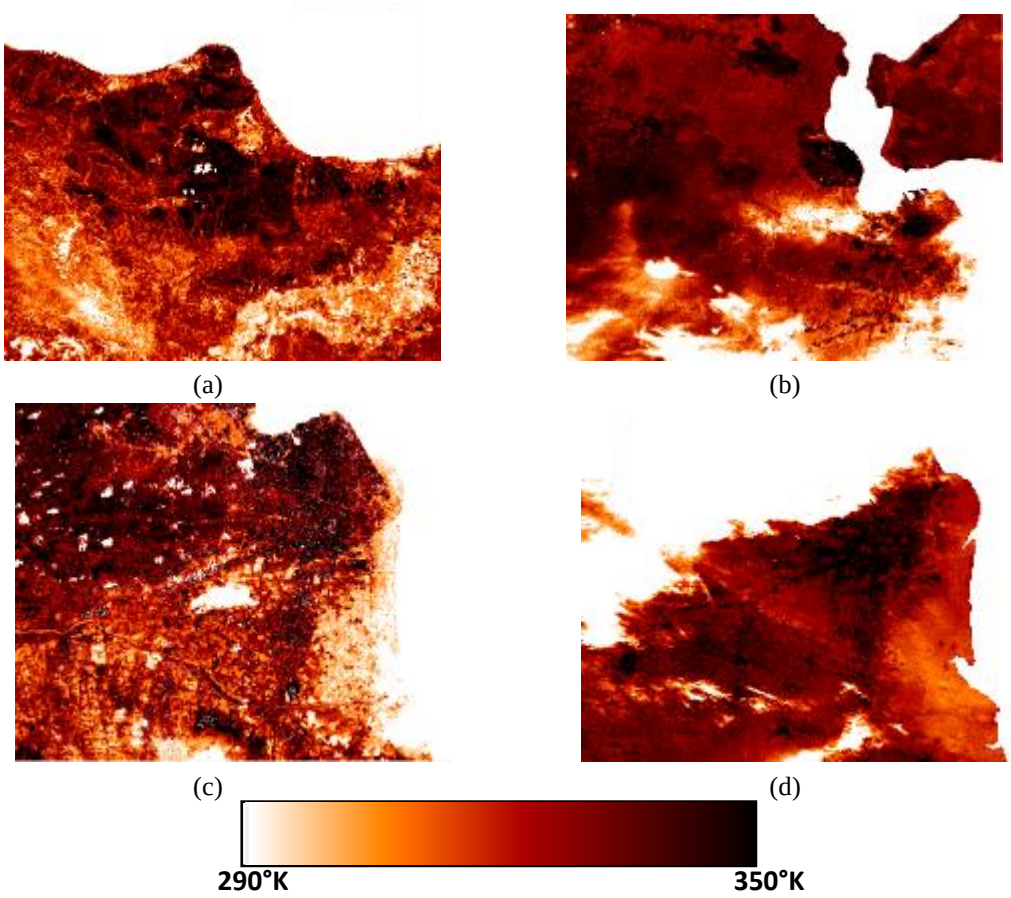

Figure 3. Other Location Result of Land Surface Temperature; (a) Landsat 7 ETM+ (02 October 2002/Tuban Regency), (b) Landsat 7 ETM+ (14 January 2013/Surabaya City), (c) Landsat 8 OLI/TIRS (03 Oktober 2014/Surabaya City) and (b) Landsat 8 OLI TIRS (07 January 2015/Surabaya City).

Land surface temperature differences on both Landsat images show that certain objects on ETM + and OLI / TIRS are up and down. Noteworthy for Landsat 7 ETM + land surface temperature values at different vegetation from Landsat 8 OLI / TIRS, because the low vegetation has lower land surface temperature value than the high one. Medium density vegetation has the highest scores on the Landsat 7 ETM + in terms of the vegetation appearance, while on Landsat 8 OLI / TIRS land surface temperature values are highly consistent to the vegetation where the low value is possessed by the high density of vegetation. The condition is also seen in bodies of water that cover the land where one of them are the water pond with water puddles on agricultural land. It proves that the processing of Landsat 8 OLI / TIRS using the SWA has consistent results with objects on land cover than Landsat 7 ETM +.

3.2. Drought Monitoring

Analyzing drought with TCI and CWSI method used an algorithm that uses input values into a land surface temperature index. Both algorithms show results of the spread of drought land cover-open class land. In dry season the drought locations are highly more visible than in the wet, however for the class of land cover types and undeveloped land is difficult to be detected as drought areas because the

condition can be caused by increasing in the land surface temperature triggered by the fumes and the lack of green area. Those conditions can be shown in the Figure 4.

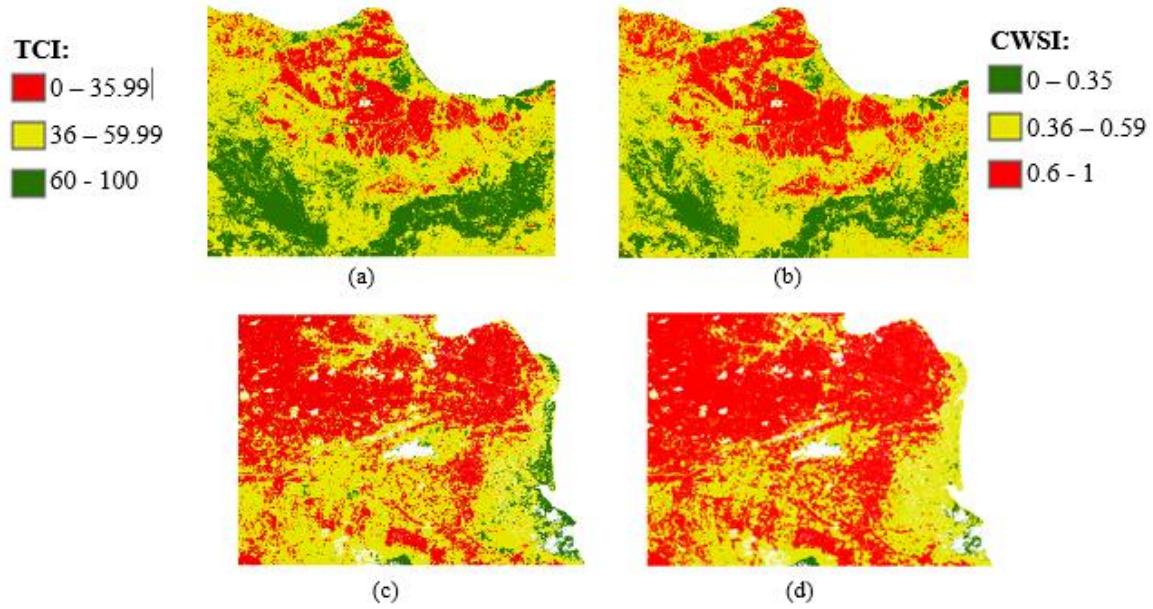

Figure 4. The Results of TCI and CWSI (a) TCI in October 2002, (b) CWSI in October 2002, (c) TCI October 2014, and (d) CWSI in October 2014.

TCI and CWSI method in 2002 showed that the detected locations have some differences. CWSI showed that the drought location is more clustered than the TCI. In 2014 the appearance of TCI and CWSI are very different due to the appearance of undeveloped land which has a dominant value of high surface temperatures. TCI in 2014 is still able to distinguish the wet location outside of Surabaya compared to CWSI. It proves that the use of TCI and CWSI methods are to adjust the location where the detection is going to be conducted.

The use of both methods proves that both have nearly identical results when they are classified. It shows that the use of algorithms for surface temperature values are still not effective, however it can be done with the combination of more complex algorithms in order to obtain the credible result. Based on the index of surface temperature of both algorithms can be seen on the Figure 5 below.

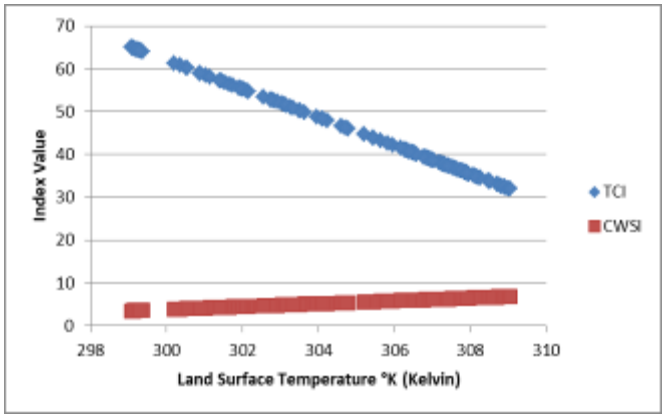

Figure 5. Diagram of Land Surface Temperature Values Based on Drought Detecting Methods (TCI and CSWI)

The curve in Figure 5 shows that the boundaries between dry and wet areas can be determined. It can be seen even if the value of the surface temperature cannot be applied on the different areas. It should be noticed that the value of the surface temperature seem to be able to distinguish drought conditions directly without having to use such a second methods. The condition is indicated by a positive relationship on figure 5 for CSWI and negative relationship for TCI.

3.3 Validation

The checking conducted on the field work is to compare the conditions in the field with the processing results. The fieldwork conducted by knowing the condition of the surrounding soil to the growing vegetation conditions (Figure 6).

(a) (b) (c)

Figure 6. The Real Condition in the Areas Correspond to the Results; (a) Karst Topography with several vegetation, (b) Built-up Area, and (c) Paddy field with crack soil.

The activities on the ground and the image recording data were carried out at different times. Therefore the exact time is unidentified. However they can be identified that they are conducted in August till October (dry months). Besides the temperature measurement is not conducted because of the different time. Therefore it is done by comparing the other images such as MODIS. On the other hand, it also cannot be done because of the cloud covering the location.

4. Conclusion

The comparison of land surface temperature processing method through Landsat 7 ETM + and 8 OLI / TIRS proves that the use of Split Windows Algorithm (SWA) method was able to show corresponding results to the conditions of land cover and has a value range which is not far each other. But it needs further research on Split Windows Algorithm (SWA) method by using several different methods based on the same data that is Landsat 8 OLI / TIRS.

Methods of drought Temperature Condition Index (TCI) and Crop Water Stress Index (CWSI) provide almost similar results on both methods. The difference of those methods is on the research sites in order to provide optimal results. On a location that has a very solid and undeveloped land is much more effective to use of TCI but if location with local conditions have varied in vegetation covering, CWSI become the best choice.

Based on the results of both methods with the value of the land surface temperature, it can be seen that the surface temperature processing is directly able to show drought conditions, although it does not use a particular method. However it still cannot be used as a reference because there are many methods for drought detection in which the surface temperature becomes an input. Researcher recommends adding many parameters to know drought monitoring like; vegetation and geomorphology condition in the area. The both parameters have an important role from identification drought on the land because they can look real in the land and have correlation with land surface temperature.

5. References

[1] Lambin E F and Ehrlich D 1997 Land-cover changes in sub-Saharan Africa (1982--1991): Application of a change index based on remotely sensed surface temperature and vegetation indices at a continental scale *Remote Sens. Environ.* **61** 181–200
[2] Adiningsih E S 2014 Tinjauan Metode deteksi parameter kekeringan berbasis data penginderaan jauh *Seminar Nasional Penginderaan Jauh.: Pengolahan Data dan Pengenalan Pola. Hlm* pp 210–20
[3] Jeyaseelan A T 2003 Droughts & floods assessment and monitoring using remote sensing and GIS *Satellite remote sensing and GIS applications in agricultural meteorology* vol 291 (World Meteorol. Org. Dehra Dun, India. Geneva, Switz)
[4] Kogan F N 1997 Global drought watch from space *Bull. Am. Meteorol. Soc.* **78** 621–36
[5] Idso S B, Jackson R D, Pinter Jr P J, Reginato R J and Hatfield J L 1981 Normalizing the stress-degree-day parameter for environmental variability *Agric. Meteorol.* **24** 45–55
[6] Coll C, Galve J M, Sanchez J M and Caselles V 2010 Validation of Landsat-7/ETM+ thermal-band calibration and atmospheric correction with ground-based measurements *IEEE Trans. Geosci. Remote Sens.* **48** 547–55
[7] Sobrino J A, El Kharraz J and Li Z-L 2003 Surface temperature and water vapour retrieval from MODIS data *Int. J. Remote Sens.* **24** 5161–82
[8] Rozenstein O, Qin Z, Derimian Y and Karnieli A 2014 Derivation of land surface temperature for Landsat-8 TIRS using a split window algorithm *Sensors* **14** 5768–80
[9] Bappeda East Java Province 2014 *Rencana Pembangunan Jangka Menengah Daerah (RPJMD) chapter 2*
[10] Robert A S 2007 Remote sensing: Models and methods for image processing *By Elsevier Inc. All rights Reserv.* p300--304
[11] Chavez Jr P S 1988 An improved dark-object subtraction technique for atmospheric scattering correction of multispectral data *Remote Sens. Environ.* **24** 459–79
[12] Qin Z, Dall'Olmo G, Karnieli A and Berliner P 2001 Derivation of split window algorithm and its sensitivity analysis for retrieving land surface temperature from NOAA-advanced very high resolution radiometer data *J. Geophys. Res. Atmos.* **106** 22655–70